Supplement to "Noise and information transmission in promoters with multiple internal states"

Georg Rieckh[1]
IST Austria,
Klosterneuburg, Austria

Gašper Tkačik
IST Austria,
Klosterneuburg, Austria

January 7, 2014

[1]Corresponding author. Address: Institute of Science and Technology Austria, Am Campus 1, A–3400 Klosterneuburg, Austria Tel.: +43(650)8415095

1 Experimentally measured promoter switching rates

Direct measurements of switching rates are rare since they require live imaging. Examples include the relative measurements of on-, off- and mRNA-production rates in *E. coli* (44) using the MS2-GFP system (72), reporting $2-10$ fold higher on- than off-rates, and mRNA production rates an order of magnitude higher than the on-rates; original bursting reported in (72) finds the on-time duration to be roughly 6 and the off time 37 minutes in a synthetic *E. coli* reporter system. Recently, on-rates of $\sim 3\cdot 10^{-2}$ min^{-1}, roughly ten-fold higher off-rates, and mRNA production rates ranging from $0-5$ min^{-1} have been reported in mammalian cells using the luciferase reporter system (59). Using new high-throughput microfluidic methods, it is now possible to measure TF binding and unbinding times directly: Ref (73) reports mouse and yeast in vitro transcription factor dissociation rates between ~ 10 s^{-1} and 10^{-2} s^{-1}, as well as the range of the corresponding association rates; it is, however, less clear if these can be unambiguously identified with switching rates in functional models.

A larger body of work extracts the rates of the two-state model from the noise characteristics (which are the primary measurement), *assuming* the two-state model without diffusion noise is applicable. The reported Fano factors for mRNA counts vary, but are of the order of $1-10$. The typical values for kinetic parameters extracted for a range of *E. coli* promoters are $10^{-3}-10^{-2}$ s^{-1} for the on-rate, $10^{-1}-1$ s^{-1} for the mRNA production rate when induced, and a variable off-rate that depends strongly on the induction level (44). Using a similar technique in mammalian cells, Raj et al (47) extracted two-state parameters and found the on-rate normalized by mRNA decay time to be roughly of order unity, while the ratio of mRNA production rate to the off-rate varied from $\sim 10-400$, depending on the system and the induction level.

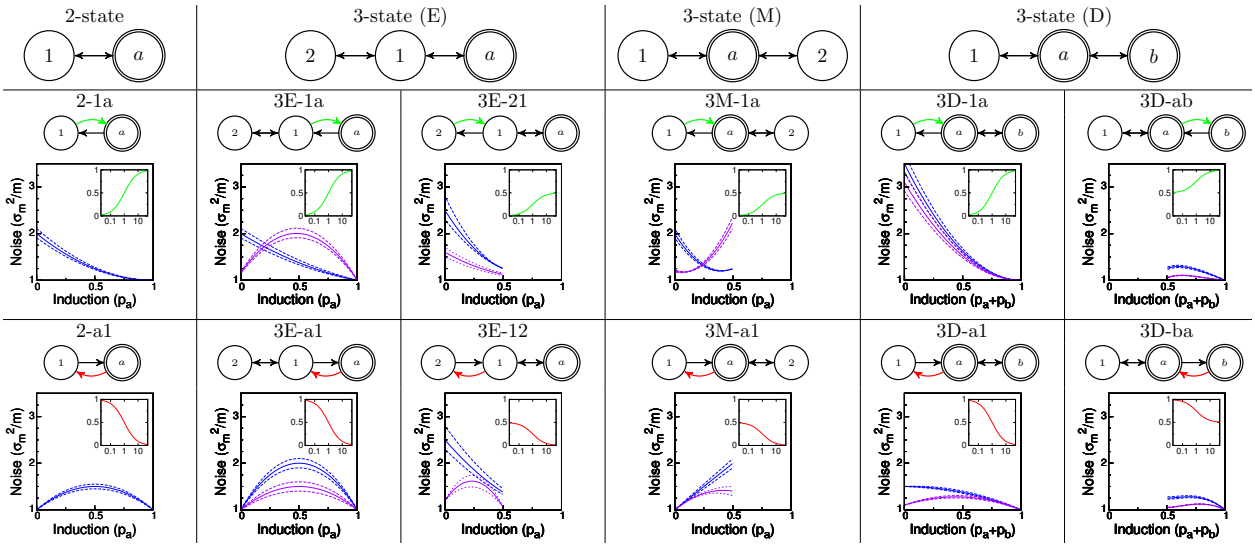

Figure S1: **Promoter architectures and interpretations. Scheme 2-1a:** (i) State a is the empty promoter (available for transcription), and state 1 corresponds to it being occupied by a repressing protein (e.g. a specific TF or a nucleosome). Mechanisms that change the rate of switching from state 1 into a (i.e. scheme 2-1a) are well documented for eukaryotic cells (69, 74). (ii) Simple activation where state 1 is the empty promoter and state a has an activating TF bound to it; changing TF concentration modulates k_{1a} (41, 52). **Scheme 2-a1:** The bacterial *lac*-promoter, where the binding of a specific TF represses expression. A change in the concentration of TFs now corresponds to modulating the rate k_{a1} and the rate k_{1a} is determined by the interaction energy between TF and its binding site (75, 76). **Scheme 3E:** (i) A promoter that has overlapping binding sites for both, an activator and a repressor (dual regulation) (48, 50, 77). Changing the concentration of the activator (repressor) leads to a change in rate k_{1a} (k_{12}), which means it can be modeled as a 3E-1a (3E-12) scheme. (ii) Eukaryotic promoters with a TATA box can be modeled as 3E-21 (71). Here, state 2 is the DNA in a state not available for transcription (closed chromatin), state 1 is the conformation where the promoter (and the TATA box) is exposed and state a corresponds to the active configuration of the DNA with the pre-initiation complex assembled. Changing the concentration of chromatin remodelers now influences the rate k_{21} (similar to the k_{1a}-modulation in the scheme 2-1a mentioned above), which yields scheme 3E-21. (iii) A coarse-grained model of DNA-looping in the *lac*-operon (78). **Scheme 3M:** A nucleosome and a specific, repressing TF compete for a promoter; changes in the input TF concentration correspond to 3M-a1, while changes in factors decreasing nucleosome occupancy correspond to 3M-1a. **Scheme 3D:** (i) State 1 is the closed chromatin formation, state a is the empty promoter and in state b a TF is bound to the DNA in such a way that it prohibits the closing of the chromatin (but still permits transciption) (79, 80). In this way, even though the input molecule does not necessarily interact with the RNA polymerase directly, it can act as an activator (or rather as a de-repressor), yielding scheme 3D-ab. (ii) A scheme used to describe any promoter where the basal expression does not follow a Poisson process (optionally with different rates of expression from a and b). (iii) Promoter with a TATA box and a competing nucleosome (cf. 3E-21) if there is a significant amount of expression from the basal state a. (iv) A scheme used as a phenomenological model with unidentified third state to explain universal noise behavior in bacterial gene expression (44, 71). Cited references use similar models.

2 Multi-state promoters as state-transition graphs

In this section we describe the general method used to derive the behavior of noise and mean for different promoter architectures, followed by a calculation for one example architecture.

2.1 Translating a state transition diagram into dynamic equations

Let $\{a, b, \dots M\}$ denote the states of the promoter that produce mRNA at a fixed rate r and $\{1, 2, \dots N\}$ denote states without production. For $\mathcal{S} = \{a, b, \dots M, 1, 2, \dots N\} \ni i, j$, let $k_{ij} \geq 0, i \neq j$ be the rate with which the promoter switches from state i to state j, d be the rate of mRNA-degradation, and p_i be the fractional occupancy of state i. For simplicity, we will only treat the case $M = 1$ here.

Deterministic equations. The list of (non-zero) rates fully defines the state-transition graph, i.e. the promoter model. This directly translates into a linear system of equations that describes the dynamics of the system:

$$\partial_t \boldsymbol{p} = \boldsymbol{K}\boldsymbol{p} \quad , \quad \text{with} \tag{1}$$

$$\boldsymbol{K} = \begin{bmatrix} -\sum_{j\in\mathcal{S}} k_{aj} & k_{1a} & \cdots & k_{Na} \\ k_{a1} & -\sum_{j\in\mathcal{S}} k_{1j} & \cdots & k_{N1} \\ \vdots & \vdots & \ddots & \vdots \\ k_{aN} & k_{1N} & \cdots & -\sum_{j\in\mathcal{S}} k_{Nj} \end{bmatrix}, \quad \boldsymbol{p} = \begin{bmatrix} p_a \\ p_1 \\ \vdots \\ p_N \end{bmatrix} \quad , \tag{2}$$

subject to the normalization constraint $\sum_{i\in\mathcal{S}} p_i = 1$.

The dynamics of mRNA are described by linking them to the activity of the promoter:

$$\partial_t m = r p_a - d m \quad . \tag{3}$$

To compute the average amount of mRNA $\bar{m}$ in steady state, we set the time derivatives to 0 and solve the linear set of equations

$$\boldsymbol{K}\bar{\boldsymbol{p}} = 0 \quad , \tag{4}$$

$$\bar{m} = \frac{r}{d} p_a \quad . \tag{5}$$

As the occupancy of the active state p_a is a function of the rates in $\boldsymbol{K}$, we can obtain the dependence of $\bar{m}$ on any rate of interest, i.e. we can obtain the regulation function.

Langevin approach to calculate noise behavior. For the noise behavior, we linearize Eqs (4,5) of the main text around the mean:

$$\boldsymbol{p}(t) = \bar{\boldsymbol{p}} + \delta p(t), \tag{6}$$

$$m(t) = \bar{m} + \delta m(t) \tag{7}$$

and introduce the Fourier-transformed variables

$$\delta p_i(t) = (2\pi)^{-1} \int d\omega \, \delta\hat{p}_i(\omega) \exp(-\mathrm{i}\omega t) \quad , \tag{8}$$

$$\delta m(t) = (2\pi)^{-1} \int d\omega \, \delta\hat{m}(\omega) \exp(-\mathrm{i}\omega t) \quad , \tag{9}$$

so that we get the linear response to random fluctuations:

$$(-\mathrm{i}\omega)\delta\hat{\boldsymbol{p}} = \boldsymbol{K}\delta\hat{\boldsymbol{p}} + \hat{\boldsymbol{\xi}} \quad , \tag{10}$$

$$(-\mathrm{i}\omega)\delta\hat{m} = r\delta\hat{p}_a - d\delta\hat{m} + \hat{\xi}_m \quad . \tag{11}$$

The statistics of the Langevin forces are given by:

$$\langle\hat{\xi}_i^*\hat{\xi}_j\rangle = -(\hat{p}_i K_{ij} + \hat{p}_j K_{ji}) \quad , \tag{12}$$

$$\langle\hat{\xi}_m^*\hat{\xi}_m\rangle = 2d\bar{m} \quad ; \tag{13}$$

to see this for the variances, consider $\langle\xi_i\xi_i^*\rangle = -2\hat{p}_i K_{ii} = 2\hat{p}_i \sum_j k_{ij}$, since all entries in the diagonal of $\boldsymbol{K}$ are negative. This is two times the rate of leaving state i. Similarly, for $\langle\xi_m^*\xi_m\rangle$ the variance is two times the rate of degrading a molecule. The factor of two comes from the fact that we consider a system at steady state, so the rates of entering and leaving a state (or creating an destroying a molecule) must be equal. For the covariances $\langle\xi_i^*\xi_j\rangle$ $(i \neq j)$, the two Langevin forces are anti-correlated, since leaving one state means entering another. The rate of changing between the two states is the probability of being in state i (p_i) times the rate of transition from that state into the other $(k_{ij} = K_{ij})$ – and this holds for both directions between the pair of states. Also, since we assume that production of mRNA and promoter switching are independent, $\langle\xi_i^*\xi_m\rangle = 0$ for all states i.

To get the variance in mRNA, we compute $\sigma_m^2 = (2\pi)^{-1}\int d\omega\,|\delta\hat{m}(\omega)|^2$, where $\delta\hat{m}(\omega)$ is obtained from Eq (11) as

$$\langle\delta\hat{m}^*\delta\hat{m}\rangle = \frac{2d\bar{m}}{d^2+\omega^2} + \frac{r^2}{d^2+\omega^2}\langle\delta\hat{p}_a^*\delta\hat{p}_a\rangle \quad , \tag{14}$$

where $\langle\delta\hat{p}_a^*\delta\hat{p}_a\rangle$ is calculated by solving Eq (10) and using the Langevin noise magnitudes from Eqs (12,13).

With the assumption $d \ll k_{ij}$, Eq (10) becomes

$$0 = \boldsymbol{K}\delta\hat{\boldsymbol{p}} + \hat{\xi} \quad , \tag{15}$$

$$\sum_i \delta\hat{p}_i = 0 \quad , \tag{16}$$

which simplifies the expressions for the $\delta\hat{p}_i$. This is because the terms with $(-i\omega)$ in the denominator (as seen in the next section in Eqs (36,37)) would give an additional, multiplicative term of the form $1/(k_{ij}^2+\omega^2)$ in Eq (14). The ω-dependence of these terms can be neglected for the integration, since for $d \ll k_{ij}$ we have

$$\frac{1}{k_{ij}^2+\omega^2}\frac{1}{d^2+\omega^2} \approx \frac{1}{k_{ij}^2}\frac{1}{d^2+\omega^2} \quad . \tag{17}$$

2.2 Example: Dual regulation (3E-1a)

We are interested in a system where the promoter of a gene can either be occupied by an activator (present at concentration a) or a repressor (present at concentration b). If it is in the active state, it produces mRNA at a constant rate r, which is later degraded at rate d.

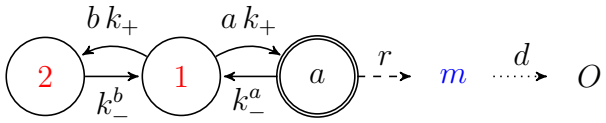

Deterministic equations. Following the setup from the last section, we translate the state transition diagram into a matrix that describes the dynamics at the promoter:

$$\begin{bmatrix} \partial_t p_a \\ \partial_t p_1 \\ \partial_t p_2 \end{bmatrix} = \begin{bmatrix} -k_-^a & ak_+ & 0 \\ k_-^a & -(ak_+ + bk_+) & k_-^b \\ 0 & bk_+ & -k_-^b \end{bmatrix} \cdot \begin{bmatrix} p_a \\ p_1 \\ p_2 \end{bmatrix} \quad . \tag{18}$$

This is then the basis for a description of the dynamics of the output (here mRNA):

$$\partial_t\, m = rp_a - dm \quad , \tag{19}$$
$$\partial_t\, p_a = ak_+ p_1 - k_-^a p_a \quad , \tag{20}$$
$$\partial_t\, p_2 = bk_+ p_1 - k_-^b p_2 \quad , \tag{21}$$
$$p_a + p_1 + p_2 = 1 \quad . \tag{22}$$

With the definitions $A = \frac{ak_+}{k_-^a}$, $B = \frac{bk_+}{k_-^b}$, $S = 1 + A + B$ and $R = \frac{r}{d}$ we get for the steady state:

$$\bar{p}_a = A/S,\ \bar{p}_1 = 1/S,\ \bar{p}_2 = B/S \quad , \tag{23}$$
$$\bar{m} = R\bar{p}_a = RA/S \quad . \tag{24}$$

Langevin approach. To see how the dynamics of the promoter influence the statistics of mRNA we perturb the systems with Langevin forces (while still keeping the gene copy number constant):

$$\partial_t\, m = rp_a - dm + \xi_m \quad , \tag{25}$$
$$\partial_t\, p_a = ak_+ p_1 - k_-^a p_a + \xi_a \quad , \tag{26}$$
$$\partial_t\, p_2 = bk_+ p_1 - k_-^b p_2 + \xi_2 \quad , \tag{27}$$
$$p_a + p_1 + p_2 = 1 \quad . \tag{28}$$

The mean of the Langevin forces is zero ($\langle \xi_i(t) \rangle = 0$) and they are uncorrelated in time ($\langle \xi_i(t)\xi_i(t') \rangle \propto \delta(t - t')$).

We linearize around the mean, where deviations from the mean are denoted by δ:

$$m(t) = \bar{m} + \delta m(t) \quad , \tag{29}$$
$$p_a(t) = \bar{p}_a + \delta p_a(t) \quad , \tag{30}$$
$$p_2(t) = \bar{p}_2 + \delta p_2(t) \quad , \tag{31}$$
$$\delta p_1(t) = -\delta p_a(t) - \delta p_2(t) \quad . \tag{32}$$

After inserting the linearized equations into the Langevin approach we perform a Fourier transform:

$$-i\omega\delta\hat{m}(\omega) = r\delta\hat{p}_a - d\delta\hat{m} + \hat{\xi}_m \quad , \tag{33}$$

$$-i\omega\delta\hat{p}_a(\omega) = ak_+\delta\hat{p}_1 - k_-^a\delta\hat{p}_a + \hat{\xi}_a \quad , \tag{34}$$

$$-i\omega\delta\hat{p}_2(\omega) = bk_+\delta\hat{p}_1 - k_-^b\delta\hat{p}_2 + \hat{\xi}_2 \quad . \tag{35}$$

Starting with the equations for the occupancies, we rewrite Eqs (34,35) and use the approximation that d is significantly slower than the other rates to get:

$$\delta\hat{p}_a(\omega) = \frac{ak_+\delta\hat{p}_1 + \hat{\xi}_a}{k_-^a - i\omega} \approx A\delta\hat{p}_1 + \frac{\hat{\xi}_a}{k_-^a} \quad , \tag{36}$$

$$\delta\hat{p}_2(\omega) = \frac{bk_+\delta\hat{p}_1 + \hat{\xi}_2}{k_-^b - i\omega} \approx B\delta\hat{p}_1 + \frac{\hat{\xi}_2}{k_-^b} \quad , \quad \text{or} \tag{37}$$

$$\delta\hat{p}_a = -\delta\hat{p}_2\frac{A}{(1+A)} + \frac{\hat{\xi}_a}{k_-^a}\frac{1}{(1+A)} \quad , \tag{38}$$

$$\delta\hat{p}_2 = -\delta\hat{p}_a\frac{B}{(1+B)} + \frac{\hat{\xi}_2}{k_-^b}\frac{1}{(1+B)} \quad . \tag{39}$$

Solving this system yields:

$$\delta\hat{p}_a = -\frac{\hat{\xi}_2}{k_-^b}\bar{p}_a + \frac{\hat{\xi}_a}{k_-^a}(\bar{p}_1 + \bar{p}_2) \quad . \tag{40}$$

The variances of the Langevin forces are:

$$\langle\hat{\xi}_a^*\hat{\xi}_a\rangle = 2k_-^a\bar{p}_a \quad , \tag{41}$$

$$\langle\hat{\xi}_2^*\hat{\xi}_2\rangle = 2k_-^b\bar{p}_2 \quad , \tag{42}$$

$$\langle\hat{\xi}_m^*\hat{\xi}_m\rangle = 2d\bar{m} \quad , \tag{43}$$

and their covariances vanish, since the direct transition from state a to state 2 is not allowed. From Eqs (33,40) we get:

$$\langle\delta\hat{p}_a^*\delta\hat{p}_a\rangle = 2\frac{\bar{p}_2}{k_-^b}\bar{p}_a^2 + 2\frac{\bar{p}_a}{k_-^a}(\bar{p}_1 + \bar{p}_2)^2 \quad , \tag{44}$$

$$\langle\delta\hat{m}^*\delta\hat{m}\rangle = \frac{2d\bar{m}}{d^2+\omega^2} + \frac{r^2}{d^2+\omega^2}\langle\delta\hat{p}_a^*\delta\hat{p}_a\rangle \quad . \tag{45}$$

Finally, with $\frac{1}{2\pi}\int_{-\infty}^{\infty} 2\frac{1}{x^2+\omega^2}\,d\omega = \frac{1}{x}$ we get:

$$\begin{aligned}\sigma_m^2 &= \frac{d\bar{m}}{d} + \frac{r^2}{d}\left(\frac{p_2}{k_-^b}p_a^2 + \frac{p_a}{k_-^a}(p_1+p_2)^2\right) = \\ &= \bar{m}\left[1 + r\left(\frac{p_2}{k_-^b}p_a + \frac{1}{k_-^a}(1-p_a)^2\right)\right] \quad .\end{aligned} \tag{46}$$

This is one description of noise in the 3E architecture. To get the noise characteristics for modulation scheme 3E-1a, we need to express p_2 in terms of p_a (not shown). From Eq (46) we can see that in the absence of repressors ($p_2 = 0$) and also for very fast unbinding of the repressors ($k^b_- \to \infty$) the noise shows the quadratic dependence on the occupation of the promoter that we see in the corresponding two-state model 2-1a.

2.3 Comparison to other methods

The results obtained with the Langevin approach were compared against two other methods: *(i)* the exact numerical solution of the chemical master equation and *(ii)* results from stochastic simulation using the Gillespie algorithm. Two kinds of comparisons are relevant: first, how well the gaussian distribution approximates the true distribution of mRNA levels; and second, how the Langevin-derived expressions for the noise characteristics compare to the exact values.

Fig S2A compares the distribution of mRNA levels obtained from the numerical solution of the chemical master equation to the gaussian approximation for the dual regulation architecture discussed in the last section.

The stochastic simulation algorithm is time consuming and offers no special benefit for the simple systems studied here, but we have nevertheless checked a few example architectures against simulation results. The results for dual regulation are shown in Fig S2B. Values for ak_+ and k^a_- were chosen from a grid. This makes it possible to show the agreement with the Langevin-derived noise characteristics in two different modulation schemes (cf. inset in Fig S2B).

Another way to obtain analytical expressions for the mean and variance of the mRNA-distributions is the method of partial moments (e.g., (48, 52)). While this method can also be used to derive higher moments, a minor advantage of the Langevin method for the purposes here is that the approximation $d \ll k_{ij}$ can be used earlier in the derivations, leading to simpler expressions.

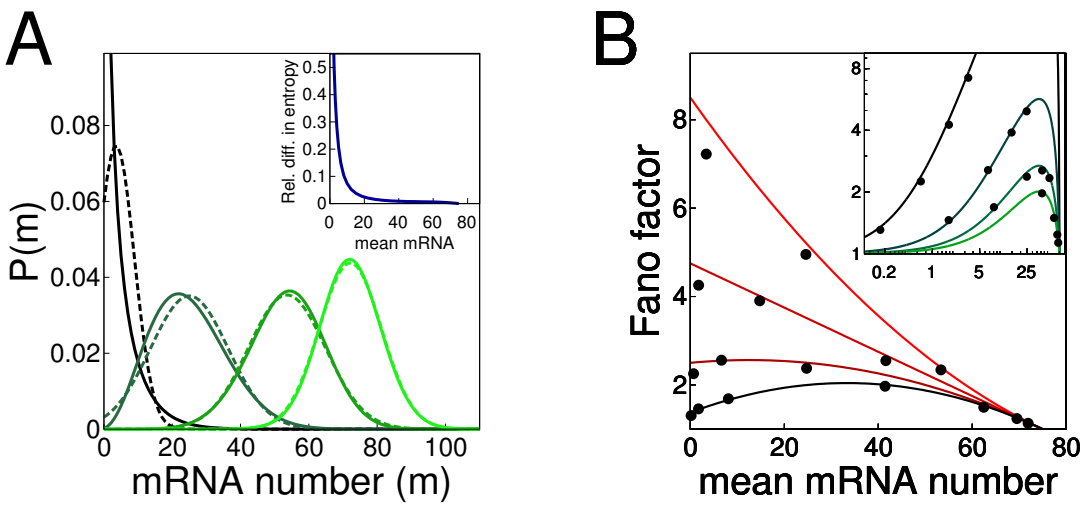

Figure S2: **Comparison of Langevin approach to other methods.** **(A)** Probability distribution of the model 3E for different values of ak_+ (thus treating it as 3E-1a). Solid lines are the numerical solution of the master equation and dashed lines are a gaussian approximation using the analytical expressions for mean and variance described in the main text. Different colors are for different values of ak_+. Parameters for this plot: $ak_+ = [1, 10, 50, 500]$, $k^a_- = 10$, $bk_+ = 10$, $k^b_- = 10$, $r = 75$ and $d = 1$. Inset: The relative difference in entropy between the full distribution and the gaussian approximation used in this study (i.e. using the results for mean and variance from the Langevin method). The error drops to $< 5\%$ very fast, with the main difference at slow rates stemming mainly from non-gaussianity at low expression levels. Importantly, for information calculations this non-gaussianity is mitigated by the protein averaging; even without the averaging, the effect on the comparison between architectures is minor. **(B)** Comparison of Fano factors for different mean expression levels for the 3E-1a model (black data points = Gillespie simulation, solid lines = Langevin method). Different colors correspond to different values for k^a_-. For small values of k^a_- and ak_+ we start to see deviations since the approximation $d \ll k_{ij}$ no longer holds. Parameters for the Gillespie simulations: $k^a_- = [10, 20, 50, 200]$, $ak_+ = [1, 10, 50, 500]$, $bk_+ = 10$, $k^b_- = 10$, $r = 75$ and $d = 1$. The Fano factor was calculated from 10000 runs. Error bars from resampling are smaller than the symbols. Inset: The same results from the Gillespie simulations replotted (on a log-log scale) and compared to the noise characteristics of the 3E-a1 scheme, i.e. the rate k^a_- is modulated to obtain different mean mRNA levels. The solid lines are the noise characteristics calculated with the Langevin methods for different (fixed) values of $ak_+ = [1, 10, 50, 500]$.

3 Magnitude of input noise

Our noise model includes the possibility of upstream noise propagating through a promoter. Two sources for this noise that is already present when the signal enters the system are considered here. The Poisson like fluctuations stemming from the production of the input molecules was already mentioned in the main text. It led to the model where input noise is propagated to the output variance in proportion to the "susceptibility" of the regulatory element:

$$\sigma_g^2 = \cdots + v \left(\frac{\partial \bar{g}}{\partial k} \right)^2 k, \tag{47}$$

where (...) indicate output and switching terms (see main text).

The second, fundamental noise source at the input side is related to the fact that the regulatory proteins need to find their interaction partners by diffusion. This puts a lower bound on the variance of the *local concentration* at the regulatory site. This diffusion limit, first formulated for the case of bacterial chemotaxis by Berg and Purcell (66), has been subsequently derived for the general case of biochemical signaling (33, 34): the lower bound on the variance in local concentration obeys $\sigma_c^2 \propto cd'/D\ell$, where D is the diffusion constant of the TF molecules, ℓ is the linear size of the binding site, and $1/d'$ is the noise averaging time (here the lifetime of the gene product). Analyses of high-precision measurements in gene expression noise during early fruit fly development have shown that this diffusion noise represents a substantial contribution to the total (35, 45). Thus, also this biophysical limit set by diffusion yields a variance that is proportional to the input itself.

To see which values the constant v can take, note that $\sigma_k^2 = k_+^2 \sigma_c^2 \propto k_+^2 cd'/D\ell = kk_+ d'/D\ell$. As an example, consider diffusion-limited association, where $k_+ = 4\pi D\ell$ (67). Depending on the accuracy and the geometry of the sensing mechanism we now get different values for $\tilde{v} = v/d'$, but in general $\tilde{v}$ is expected to be of order unity. For example, the perfect absorbing sphere has $\sigma_c^2 = cd'/(4\pi D\ell)$ and therefore $\tilde{v} = 1$; the perfect monitoring sphere in the Berg–Purcell limit has $\sigma_c^2 = 3cd'/(5\pi D\ell)$ and therefore $\tilde{v} = 2.4$ (66, 68).

References

33. Bialek, W., and S. Setayeshgar, 2005. Physical limits to biochemical signaling. *Proc Natl Acad Sci USA* 102:10040–5.

34. Bialek, W., and S. Setayeshgar, 2008. Cooperativity, sensitivity, and noise in biochemical signaling. *Phys Rev Lett* 100:258101.

35. Gregor, T., D. Tank, E. Wieschaus, and W. Bialek, 2007. Probing the limits to positional information. *Cell* 130:153–64.

41. Kepler, T., and T. Elston, 2001. Stochasticity in transcriptional regulation: origins, consequences, and mathematical representations. *Biophys J* 81:3116–36.

44. So, L.-H., A. Ghosh, C. Zong, L. Sepulveda, R. Segev, and I. Golding, 2011. General properties of transcriptional time series in Escherichia coli. *Nat Genet* 43:554–60.

45. Tkačik, G., T. Gregor, and W. Bialek, 2008. The role of input noise in transcriptional regulation. *PLoS ONE* 3:e2774.

47. Raj, A., C. Peskin, D. Tranchina, D. Vargas, and S. Tyagi, 2006. Stochastic mRNA synthesis in mammalian cells. *PLoS Biol* 4:e309.

48. Sanchez, A., and J. Kondev, 2008. Transcriptional control of noise in gene expression. *Proc Natl Acad Sci USA* 105:5081–6.

50. Karmakar, R., 2010. Conversion of graded to binary response in an activator-repressor system. *Phys Rev E* 81:021905.

52. Sanchez, A., H. Garcia, D. Jones, R. Phillips, and J. Kondev, 2011. Effect of promoter architecture on the cell-to-cell variability in gene expression. *PLoS Comput Biol* 7:e1001100.

59. Suter, D., N. Molina, D. Gatfield, K. Schneider, U. Schibler, and F. Naef, 2011. Mammalian genes are transcribed with widely different bursting kinetics. *Science* 332:472–4.

66. Berg, H., and E. Purcell, 1977. Physics of chemoreception. *Biophys J* 20:193–219.

67. Berg, O. G., and P. H. von Hippel, 1985. Diffusion-controlled macromolecular interactions. *Annu Rev Biophys Biophys Chem* 14:131–58.

68. Endres, R. G., and N. S. Wingreen, 2008. Accuracy of direct gradient sensing by single cells. *Proc Natl Acad Sci USA* 105:15749–54.

69. Carey, L. B., D. van Dijk, P. M. Sloot, J. A. Kaandorp, and E. Segal, 2013. Promoter sequence determines the relationship between expression level and noise. *PLoS Biol* 11:e1001528.

71. Sanchez, A., S. Choubey, and J. Kondev, 2013. Regulation of noise in gene expression. *Annu Rev Biophys* 42:469–91.

72. Golding, I., J. Paulsson, S. Zawilski, and E. Cox, 2005. Real-time kinetics of gene activity in individual bacteria. *Cell* 123:1025–36.

73. Geertz, M., D. Shore, and S. J. Maerkl, 2012. Massively parallel measurements of molecular interaction kinetics on a microfluidic platform. *Proc Natl Acad Sci USA* 109:16540–5.

74. Vinuelas, J., G. Kaneko, A. Coulon, E. Vallin, V. Morin, C. Mejia-Pous, J.-J. Kupiec, G. Beslon, and O. Gandrillon, 2013. Quantifying the contribution of chromatin dynamics to stochastic gene expression reveals long, locus-dependent periods between transcriptional bursts. *BMC Biol* 11:15.

75. Sanchez, A., M. L. Osborne, L. J. Friedman, J. Kondev, and J. Gelles, 2011. Mechanism of transcriptional repression at a bacterial promoter by analysis of single molecules. *EMBO J* 30:3940–6.

76. Garcia, H., A. Sanchez, J. Boedicker, M. Osborne, J. Gelles, J. Kondev, and R. Phillips, 2012. Operator sequence alters gene expression independently of transcription factor occupancy in bacteria. *Cell Rep* 2:150–61.

77. Yang, H.-T., and M. S. H. Ko, 2012. Stochastic modeling for the expression of a gene regulated by competing transcription factors. *PLoS ONE* 7:e32376.

78. Earnest, T. M., E. Roberts, M. Assaf, K. Dahmen, and Z. Luthey-Schulten, 2013. DNA looping increases the range of bistability in a stochastic model of the lac genetic switch. *Phys Biol* 10:026002.

79. Mirny, L., 2010. Nucleosome-mediated cooperativity between transcription factors. *Proc Natl Acad Sci USA* 107:22534–9.

80. Segal, E., and J. Widom, 2009. What controls nucleosome positions. *Trends Genet* 25:335–42.